energies

MDPI

Article

Characterization of Stages of CO_2-Enhanced Oil Recovery Process in Low-Permeability Oil Reservoirs Based on Core Flooding Experiments

Yutong Zhu [1,2], Xinwen Wang [1,2,3], Yulong Kang [4,*], Chaobin Guo [1,2], Qingcheng He [1,2] and Cai Li [1,2,*]

[1] Chinese Academy of Geological Sciences, Beijing 100037, China; zhuyt2024@126.com (Y.Z.); wangxinwen97@126.com (X.W.); guochaobin@cags.ac.cn (C.G.); heqc@cags.ac.cn (Q.H.)
[2] Technology Innovation Center for Carbon Sequestration and Geological Energy Storage, Ministry of Natural Resources, Beijing 100037, China
[3] School of Water Resources and Environment, China University of Geosciences, Beijing 100083, China
[4] Shaanxi Yanchang Petroleum (Group) Co., Ltd., Xi'an 710075, China
* Correspondence: kangy2@foxmail.com (Y.K.); licai@cags.ac.cn (C.L.)

Abstract: Understanding the CO_2 displacement mechanism in ultra-low-permeability reservoirs is essential for improving oil recovery. In this research, a series of displacement experiments were conducted on sandstone core samples from the Chang 6 reservoir in the Huaziping area using a multifunctional core displacement apparatus and Nuclear Magnetic Resonance (NMR) technology. The experiments were designed under conditions of constant pressure, variable pressure, and constant effective confining stress to simulate various reservoir scenarios. The results indicated that the distribution characteristics of the pore structure in the rock samples significantly influenced the CO_2 displacement efficiency. Specifically, under identical conditions, rock cores with a higher macropore ratio exhibited a significantly enhanced recovery rate, reaching 68.21%, which represents a maximum increase of 31.97% compared to cores with a lower macropore ratio. Though fractures can facilitate CO_2 flowing through pores, the confining pressure applied during displacement caused a partial closure of fractures, resulting in reduced rock permeability. Based on the oil-to-gas ratio and oil recovery in the outlet section of the fractured rock samples, the CO_2 displacement process exhibited five stages of no gas, a small amount of gas, gas breakthrough, large gas channeling, and gas fluctuation. Although the displacement stage of different cores varies, the breakthrough stage consistently occurs within the range of 2 PV. These insights not only enhance our understanding of CO_2 displacement mechanisms in low-permeability reservoirs but also provide actionable data to inform the development of more effective CO_2-EOR strategies, significantly impacting industrial practices.

Keywords: low permeability; Chang 6 reservoir; CO_2 flooding; NMR; oil recovery

check for updates

Citation: Zhu, Y.; Wang, X.; Kang, Y.; Guo, C.; He, Q.; Li, C. Characterization of Stages of CO_2-Enhanced Oil Recovery Process in Low-Permeability Oil Reservoirs Based on Core Flooding Experiments. *Energies* **2024**, *17*, 5469. https://doi.org/10.3390/en17215469

Academic Editor: Hossein Hamidi

Received: 1 October 2024
Revised: 26 October 2024
Accepted: 28 October 2024
Published: 31 October 2024

Copyright: © 2024 by the authors. Licensee MDPI, Basel, Switzerland. This article is an open access article distributed under the terms and conditions of the Creative Commons Attribution (CC BY) license (https://creativecommons.org/licenses/by/4.0/).

1. Introduction

The global energy demand is expected to grow by about 25% over the next decade [1]. According to the International Energy Agency's World Energy Outlook 2023, despite the expansion of renewable energy sources, fossil fuel consumption has not decreased and continues to rise in response to the growing global energy demand [2]. Petroleum, as a fundamental raw material in the chemical industry, remains in high demand due to its irreplaceable role in various sectors and its critical function as a feedstock for chemicals and materials [3]. China's oil reserves are dominated by low-permeability reservoirs. The ultimate oil recovery rate of low-permeability reservoirs is much lower than 35%, the global average [4]. As one of enhanced oil recovery (EOR) technologies and also a carbon storage option, CO_2-EOR is double beneficial to oil reservoirs [5]: not only enhancing oil recovery but also allowing for long-term geological storage of CO_2 to mitigate climate

change [6]. However, low injectivity poses many challenges for CO_2-EOR application in low-permeability oil reservoirs [7,8].

In recent years, significant progress has been made in CO_2-enhanced oil recovery technology for improving the recovery rate in low-permeability oil reservoirs. For instance, Gong and Gu (2015) showed that CO_2-EOR can significantly improve oil and gas recovery rates in sandstone and carbonate reservoirs, although fractures may reduce its efficiency [9]. Additionally, Wang et al. (2017) found that during the CO_2-EOR process in ultra-low-permeability reservoirs, phenomena such as gas breakthrough and the formation of extensive gas channels often occur, necessitating improved injection strategies [10]. Experimental research by Zhou et al. (2019) emphasized that the micro-pore characteristics of rocks, such as pore size distribution and connectivity, are critical factors determining the success of CO_2-EOR [11]. Furthermore, research by Han et al. (2021) showed that the density and distribution of fracture networks directly affect the flow paths of CO_2 and ultimately the efficiency of oil recovery [12]. Liu and Zhang (2015) indicated through simulation studies that adjustments in the pressure and rate of CO_2 injection can effectively control gas breakthrough, thereby enhancing recovery rates in low-permeability reservoirs [13]. Similarly, Abedini and Torabi (2014) conducted a series of experiments with cyclic CO_2 injections, pointing out that cyclic injections can significantly enhance the storage potential of CO_2 in reservoirs, as well as increase crude oil recovery [14]. Li et al. (2018) determined the diffusion coefficients of supercritical CO_2 under tight reservoir conditions using the pressure decay method, providing important data for optimizing CO_2-EOR technology [15].

Despite these advances, comprehensive and quantitative studies on the effects of CO_2 flooding under different physical and geological conditions are still insufficient. Existing studies have mostly focused on specific conditions, such as gas breakthrough and fracture networks, but lack systematic quantitative analysis and in-depth mechanism exploration. In addition, the CO_2 displacement efficiency at different stages in low-permeability reservoirs has not been fully characterized. These research gaps highlight the need for further research on the underlying mechanisms that control CO_2 flow and displacement efficiency in such reservoirs [16–19]. In response to the above issues, we analyzed the CO_2 displacement process in low-permeability reservoirs using Nuclear Magnetic Resonance (NMR) technology, particularly exploring the characteristics of displacement efficiency at different injection stages. The oil displacement behavior of CO_2 in low-permeability reservoirs and its impact on displacement efficiency are studied. The characteristics and efficiency of different displacement stages of the CO_2 displacement process in low-permeability reservoirs are quantitatively described. This research not only enhances understanding of the CO_2 oil displacement mechanism in low-permeability reservoirs but also provides quantitative data and analysis for optimizing development strategies, significantly impacting industrial practices.

2. Methodology

2.1. Research Area

The Chang 6 reservoir of the Yanchang Formation in the Huaziping area is characterized as a typical low-permeability lithologic reservoir, primarily driven by elastic and dissolved gas mechanisms, with no significant bottom or edge water present. The oil-bearing region spans an area of 28.27 km^2 and has geological reserves estimated at 14.6 million tons. Figure 1 shows the location map of the research area. The reservoir temperature is measured at 46 °C, with an initial formation pressure of 8.9 MPa and a current formation pressure of 5.2 MPa. The average reservoir thickness is 14.10 m, and the average porosity ranges from 7% to 12%. The permeability is recorded at 0.94×10^{-3} μm^2, while the average oil saturation is 42.2%. The formation crude oil exhibits a density of 0.79 g/cm^3 and a viscosity of 3.4 MPa·s, with an average wax content of 10.46%. The formation water is of the $CaCl_2$ type, with salinity ranging between 32.14 and 79.39 g/L.

The Chang 6 layer is overlain by the Chang 4 + 5 caprock, which has a thickness ranging from 70 to 90 m.

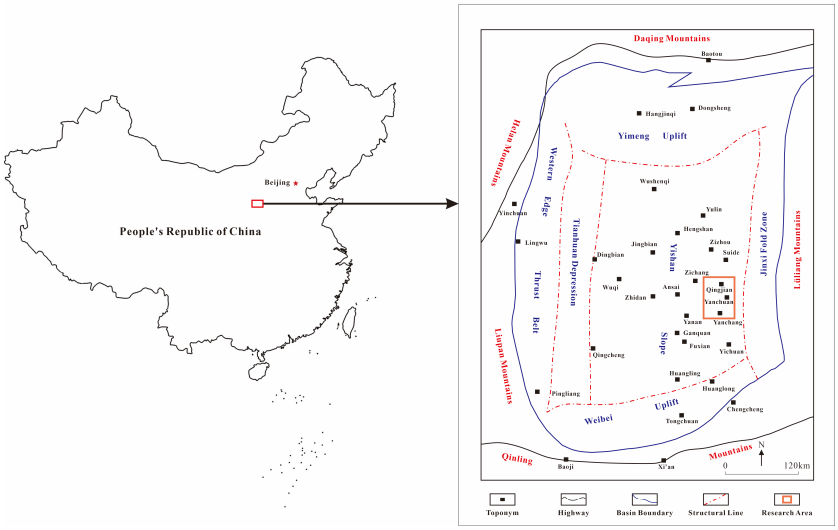


Figure 1. Location map of the research area.

The area currently hosts 385 production wells and 100 water injection wells, developed using an approximate inverse nine-spot well pattern. During the initial production phase, the average daily oil production per well was 2.0 tons, accompanied by a water cut of 10%. Presently, the average daily oil production per well stands at 0.5 tons, with a water cut of 36.3%. The cumulative recovery factor is recorded at 7.11%, and the injection–production ratio is 0.51.

The reservoir rock is predominantly composed of gray and light gray fine-grained feldspathic sandstone, with some sections exhibiting medium-fine to fine-grained lithic feldspathic sandstone. The average quartz content is 22.81%, while feldspar fragments constitute 52.49%, and rock fragments account for 12.68%. The sandstone exhibits a predominantly fine-grained structure, with no coarse sandstone or conglomerate observed. The primary types of cementation are pore-filling and contact cements, mainly comprising calcite and authigenic minerals. The matrix consists primarily of chlorite and montmorillonite, with minor occurrences of pyrite and bitumen. During diagenesis, the Chang 6 reservoir developed various pore types, including primary residual intergranular pores, dissolution intergranular pores, micropores, and microfractures. Overall, the sandstone is characterized by a fine-grained structure, with no coarse sandstone or conglomerate observed.

2.2. Material

The nine core samples used in the experiment were obtained from the Yanchang Formation at depths of 1200 to 1500 m in the Xingzichuan oilfield, located in the Huaziping area, Ansai County, Shaanxi Province (Table 1).

Table 1. Basic information on sandstone samples.

Sample Number	Well Number	Depth Interval (m)	Confining Pressure
5-3	HCC-38	1414.18–1415.97	18
6-1	HCC-38	1417.76–1418.48	18
5-8 (fractured)	HCC-38	1415.97–1417.76	18
5-7	HCC-38	1414.18–1415.97	20
1-1	147-CC	1280.39–1282.24	20
1-2 (fractured)	147-CC	1280.39–1282.24	20
5-2	HCC-38	1414.18–1415.97	8-12-14
6-2	HCC-38	1417.76–1418.48	18
2-2 (fractured)	147-CC	1282.24–1284.25	18

2.3. Equipment

The Oxford-MARAN DRX 2 Nuclear Magnetic Resonance (NMR) instrument, Oxford, UK (Figure 2), produced in the UK, is used to measure NMR parameters such as the longitudinal and transverse relaxation times of rocks under a constant magnetic field. The instrument's key performance specifications are as follows: (1) resonance frequency of 2 MHz; (2) magnetic field strength of 470 Gauss; (3) magnetic field homogeneity of 100 ppm; (4) minimum echo spacing of 75 μs/200 μs; and (5) a maximum echo count of 100,000.

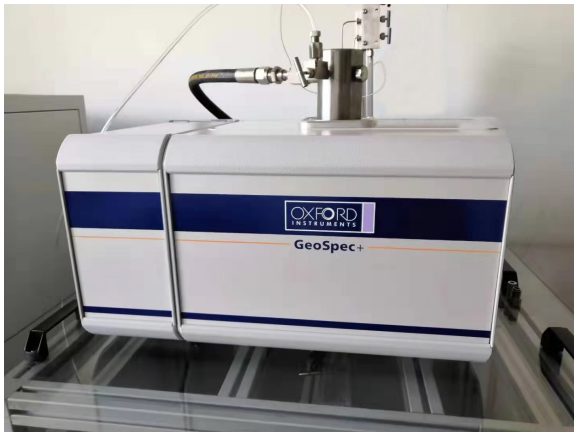


Figure 2. The Oxford-MARAN DRX 2 Nuclear Magnetic Resonance (NMR) instrument.

The synchronous core displacement NMR system comprises an oil injection system, a gas injection system, a confining pressure and temperature control system, a core holder system, a radio frequency and signal processing system, and a displacement outlet control system. The oil and gas injection systems provide displacement pressure to the samples, capable of reaching up to 70 MPa. A specialized non-magnetic core holder is employed within the core holder system, where the internal fluorine oil pressure is precisely regulated by the confining pressure and temperature control system. The radio frequency and signal processing system is responsible for signal collection and data processing. The displacement outlet control system applies outlet-end displacement pressure to the sample, effectively simulating reservoir displacement conditions. A schematic of the experimental setup is shown in Figure 3.

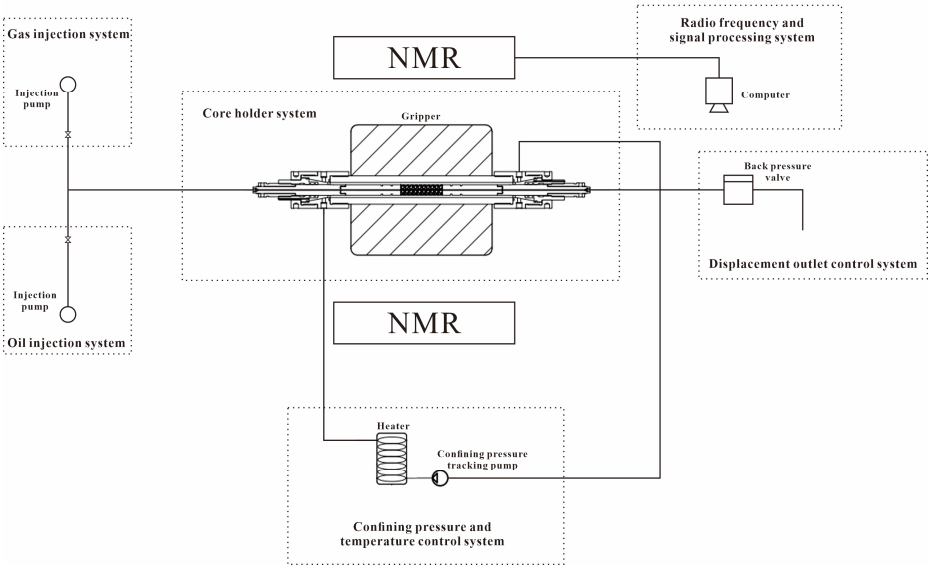


Figure 3. Schematic diagram of the experimental setup.

2.4. Experimental Principles

Nuclear Magnetic Resonance (NMR) technology fundamentally involves the acquisition and processing of proton-based information, as depicted in Figure 4 [20]. Prior to NMR analysis, protons in the sample's fluid are typically randomly oriented. At the onset of testing, a constant magnetic field is applied, aligning the protons along the direction of the magnetization vector. This is followed by an alternating electromagnetic field, inducing proton precession. Upon removal of all magnetic fields, the protons gradually return to their equilibrium state—a process termed relaxation. During relaxation, a CPMG (Carr–Purcell–Meiboom–Gill) sequence is employed to generate a series of spin echoes, collectively forming the raw NMR data (see Figure 4c). Through fitting these raw data, a T2 relaxation time distribution curve is obtained, providing critical physical parameters for fluid property analysis.

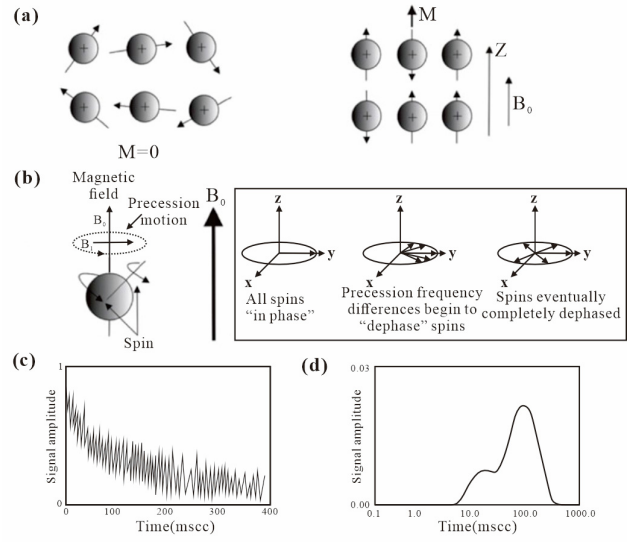


Figure 4. The complete process of NMR testing: (**a**) proton alignment, (**b**) proton precession, (**c**) raw data, (**d**) processed data.

In porous media, the transverse relaxation time T_2 consists of three components, i.e., diffusion relaxation time T_{2D}, bulk relaxation time T_{2B}, and surface relaxation time T_{2S}, which can be represented as follows:

$$\frac{1}{T_2} = \frac{1}{T_{2D}} + \frac{1}{T_{2B}} + \frac{1}{T_{2S}} \tag{1}$$

When a single fluid occupies the pore space, the contributions of diffusion relaxation time and bulk relaxation time are negligible, leading to

$$\frac{1}{T_2} \approx \frac{1}{T_{2S}} = \rho_2 \left(\frac{S}{V} \right) \tag{2}$$

where ρ_2 represents the surface relaxivity and $\frac{S}{V}$ is the specific surface area of the pore.

The specific surface area is closely related to pore structure. For pore geometries that can be simplified as spherical pores or cylindrical tubes, the specific surface area is linearly proportional to pore size, expressed as

$$\frac{1}{T_2} \approx \rho_2 \left(\frac{F_s}{rc} \right) \tag{3}$$

where F_s is the pore shape factor and rc is the mean pore radius. For a fixed pore structure, F_s remains constant. Evidently, the pore radius is directly proportional to the T_2 value,

establishing a one-to-one correspondence. Therefore, the T_2 distribution can be utilized to evaluate pore size and pore size distribution.

In practical experiments, the data collected from NMR measurements provide a distribution curve of T_2 relaxation times. This T_2 distribution can be transformed into a pore size distribution through an inversion process. Typically, a multi-exponential decay model is employed to characterize signal decay over time, expressed as

$$M(t) = \sum_i A_i e^{-\frac{t}{T_{2,i}}} \quad (4)$$

where $M(t)$ represents the signal intensity at time t; $T_{2,i}$ denotes the i-th relaxation time constant; and A_i corresponds to the signal amplitude associated with each relaxation time, indicating the volume fraction of the pore size class corresponding to $T_{2,i}$.

Through the inversion process, the T_2 relaxation time distribution A_i is mapped to corresponding pore sizes r_i, thereby yielding a quantitative pore size distribution.

2.5. Experimental Procedure

(1) The sample was placed in an oven to dry for 48 h and then weighed. The core permeability was determined using a gas drive method.

(2) The core sample was evacuated and saturated with formation water, after which it was weighed again. The porosity was calculated based on the ratio of the water volume in the core to the core volume. NMR detection was performed to obtain the T2 spectrum of the water-saturated core sample to determine the pore distribution within the core.

(3) Crude oil was injected into the water-saturated core sample at a constant rate of 0.02 mL/min. Once oil saturation was achieved, NMR detection was performed again to obtain the T2 spectrum of the oil-saturated core sample to determine the initial oil saturation.

(4) The core sample was wrapped in heat shrink tubing and placed into the core holder. The screws at both ends of the holder were tightened to secure the core, which was set at a formation temperature of 46 °C. NMR testing was conducted to obtain the initial T2 relaxation spectrum and the image of the saturated oil core.

(5) The gas injection device was started, and CO_2 was injected into the core at a constant or variable pressure. Throughout the oil displacement process, the oil displacement pressure differential and oil recovery rate were recorded in real time until no more oil was produced at the production end. (Due to the ultra-low permeability of some rock samples, the difficulty of displacement was increased. During the experiment, the CO_2 injection pressure was 16~20 MPa to ensure effective displacement.)

(6) Following the oil displacement test, NMR testing was conducted once more to obtain the T2 relaxation spectrum and the core image of the remaining oil. The oil saturation before and after CO_2 displacement was calculated using the area method on each T2 spectrum.

(7) The gas injection device was shut off, the gas control valve was opened to release the injection pressure, the pressure was adjusted to reduce it to 0 MPa, and the core sample was removed from the core holder.

To study the effect of different core permeabilities on CO_2 oil displacement efficiency, core samples with the same dimensions but different permeabilities were selected and the above experimental operations (steps 1 to 7) were repeated to conduct displacement experiments.

3. Results and Discussion

3.1. Pore Distribution

In the NMR experiments, the T2 spectrum is of significant value in characterizing oil saturation and multiphase flow [21,22]. Based on the literature [23], the correlation between T2 relaxation time and pore size was calculated. The pore size distribution of the rock samples is shown in Figure 5, with the samples primarily consisting of micropores (0–1 μm). The volume ratios of micropores for cores 5-3, 6-1, 5-8, 5-7, 1-1, 1-2, 5-2, 6-2,

and 2-2 are 98.82%, 93.80%, 98.98%, 97.52%, 78.17%, 99.39%, 99.17%, 78.91%, and 98.54%, respectively; the CO_2 displacement efficiencies are 36.55%, 40.23%, 47.05%, 49.30%, 59.70%, 43.45%, 36.24%, 68.21%, and 36.94%, respectively. The measured porosity and permeability of the cores are shown in Table 2. Among them, cores 5-3, 5-7, and 5-2 are tight cores, cores 6-1, 1-1, and 6-2 are ultra-low-permeability cores, and fractured cores 5-8, 1-2, and 2-2 are extremely low-permeability cores. Compared to previous studies, the cores used in this experiment have a higher volume proportion of micropores, with most reaching over 90% [24,25]. This significant difference is attributed to the specific types of rock samples selected and the unique characteristics of the formation.

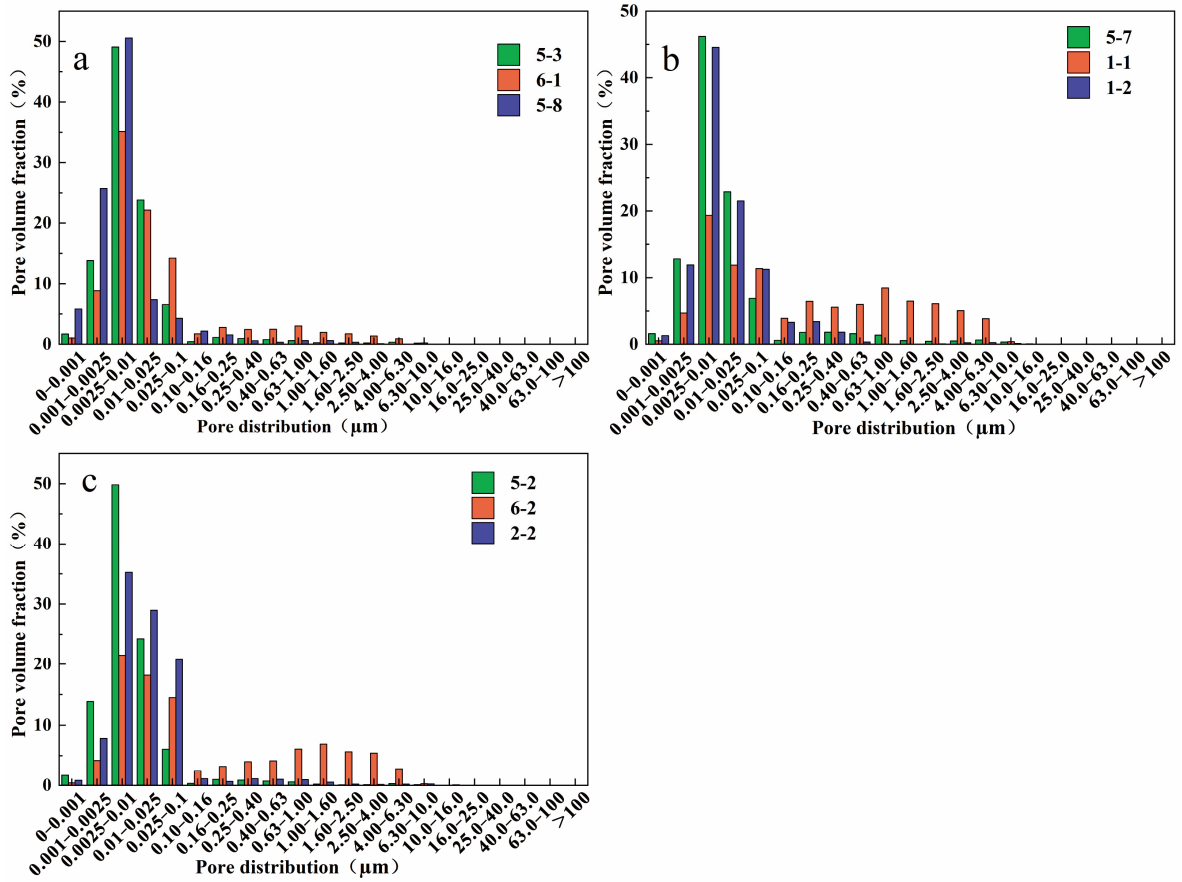


Figure 5. Core pore distribution. (**a**) constant pressure injection condition, (**b**) variable pressure injection condition, (**c**) constant effective stress injection condition.

Table 2. Porosity and permeability information of sandstone samples in gas injection experiments.

Gas Injection Conditions	Sample Number	NMR Porosity %	Measured Permeability (10^{-15} m^2)
Constant-Pressure (16 MPa) Injection	5-3	4.48	0.0024
	6-1	3.80	0.5892
	5-8	7.98	6.6932 (fractured)
Variable-Pressure (16-18-20 MPa) Injection	5-7	5.25	0.0266
	1-1	8.39	0.7540
	1-2	4.08	5.4571 (fractured)
Constant Effective Stress (2 MPa) Injection	5-2	4.58	0.0037
	6-2	8.96	0.8971
	2-2	6.01	4.3784 (fractured)

The analysis of Figure 6 reveals that in core samples with a high proportion of micropores, the oil displacement efficiency of CO_2 is significantly reduced. Compared to macropores, fluids within microporous structures encounter greater resistance during migration, preventing the formation of continuous fluid flow pathways [26]. Therefore, a higher proportion of micropores in the experiment was associated with lower oil displacement efficiency [27]. A high-volume proportion of micropores not only reduces the effective displacement efficiency of CO_2 but also significantly affects the dynamic characteristics of fluid flow. Specifically, the microporous structure, characterized by its larger specific surface area and higher fluid retention capacity, increases the contact area between the fluid and the pore walls, leading to stronger capillary forces that further impede CO_2 displacement efficiency [28]. Moreover, the small size of the micropores restricts the dynamic migration of fluids, which negatively impacts the diffusion and replacement of CO_2, thereby hindering the smooth passage of fluids [29].

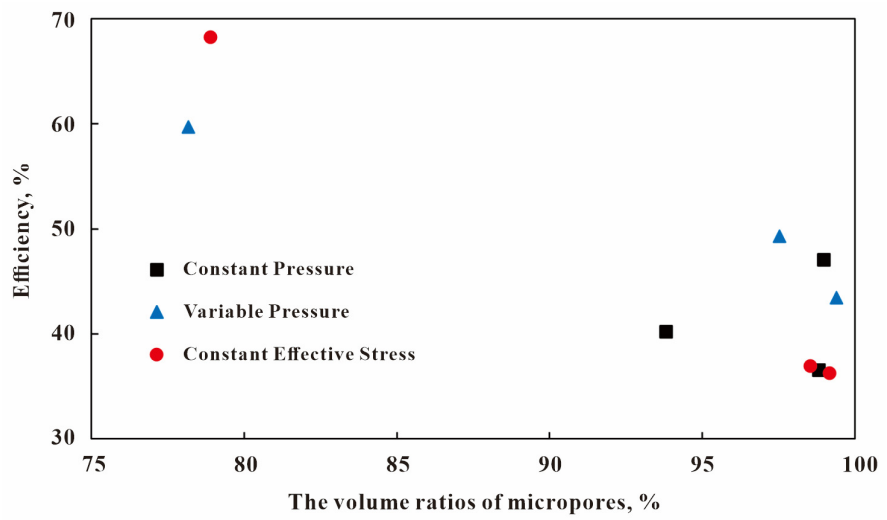


Figure 6. Micropore volume ratios and CO_2 displacement efficiency across various displacement conditions.

Under identical conditions, rock cores with a higher macropore ratio exhibited a significantly enhanced recovery rate, reaching 68.21%, which represents a maximum increase of 31.97% compared to cores with a lower macropore ratio. This finding suggests that, when CO_2 is used as a displacement medium, selecting rocks with a higher proportion of macropores can significantly improve recovery efficiency. This insight provides valuable guidance for formulating enhanced oil recovery (EOR) strategies in actual reservoirs: in formations with abundant micropores, a simple CO_2 injection may not achieve the desired displacement effect, especially in low-permeability, tight oil reservoirs. Therefore, to attain higher recovery rates, it may be necessary to incorporate additional techniques [30].

3.2. T2 Spectra Change During Core Flooding

When CO_2 displaces oil in the core, the T2 spectrum is used to dynamically monitor changes in oil flow and the distribution of residual oil. Based on previous studies [24,31], the horizontal coordinate intervals in the T2 spectrum are defined as follows: <1 ms is defined as the micropore region, 1–10 ms as the small pore region, 10–100 ms as the medium pore region, and 100–1000 ms as the large pore region. Additionally, since the oil in the fracture experiences less force from the solid surface of the core compared to the oil in the matrix, the relaxation time of oil in the fractures is longer. Moreover, the displacement process of CO_2 in fractured cores is more complex. Therefore, more T2 spectrum measurements were taken in the fractured cores to observe the microscopic changes within them.

As shown in Figures 7–9, the T2 spectra of the cores in the residual oil state under constant pressure, variable pressure, and constant effective stress conditions exhibit sig-

nificant fluctuations with the increase in injection volume. Compared to the initial state, the amplitude of the T2 spectrum gradually decreases with the increase in CO_2 injection volume, and the T2 spectrum in the micropore region of all cores decreases significantly, indicating that oil is displaced to varying degrees from the cores [32]. Under constant injection pressure conditions, the micropore region contributes significantly to the recovery rate; under variable injection pressure and constant effective stress conditions, the medium pore region also contributes significantly to the recovery rate [33].

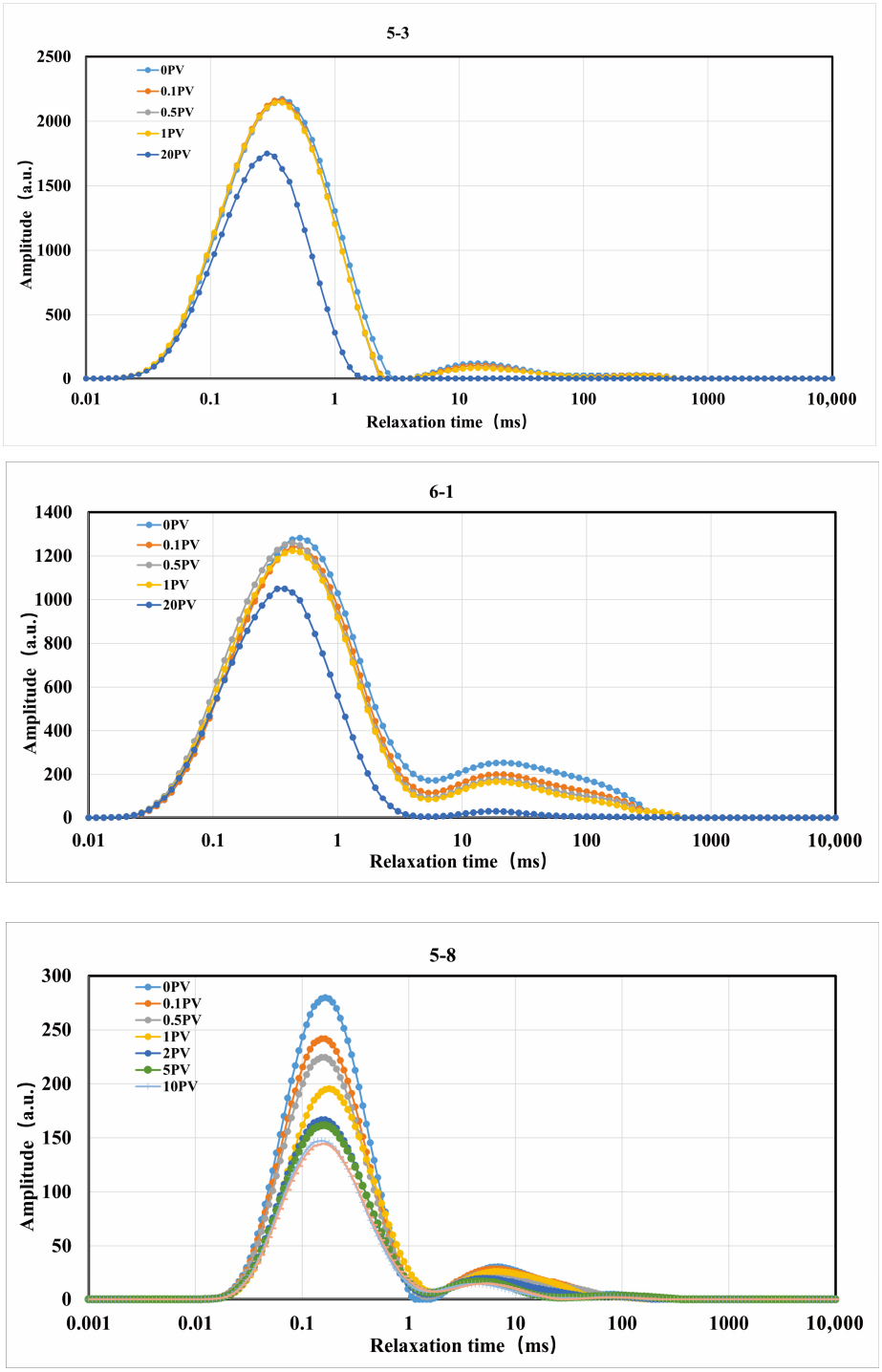


Figure 7. T2 spectrum variation of rock samples during displacement under constant injection pressure conditions.

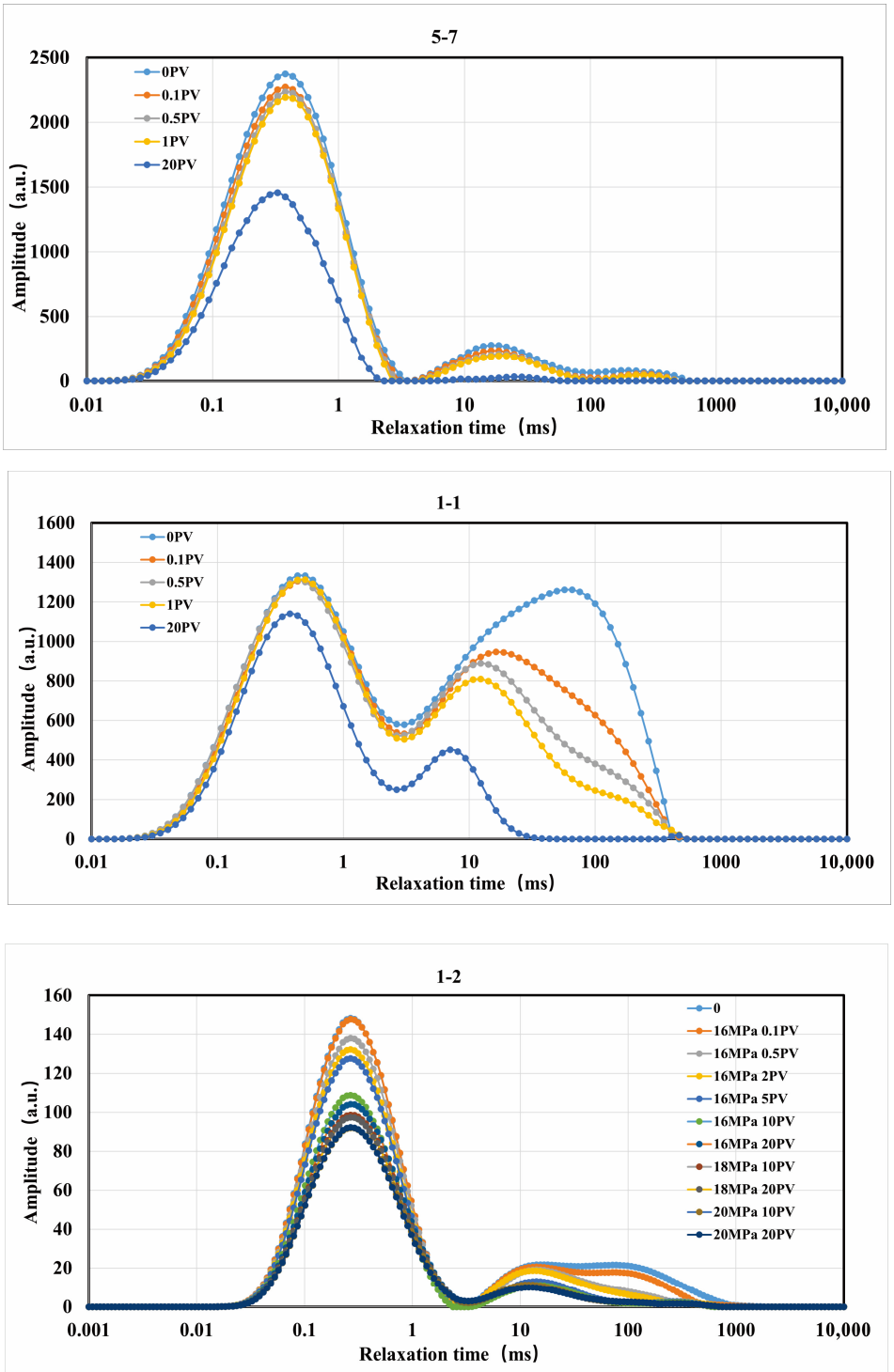


Figure 8. T2 spectrum variation of rock samples during displacement under variable injection pressure conditions.

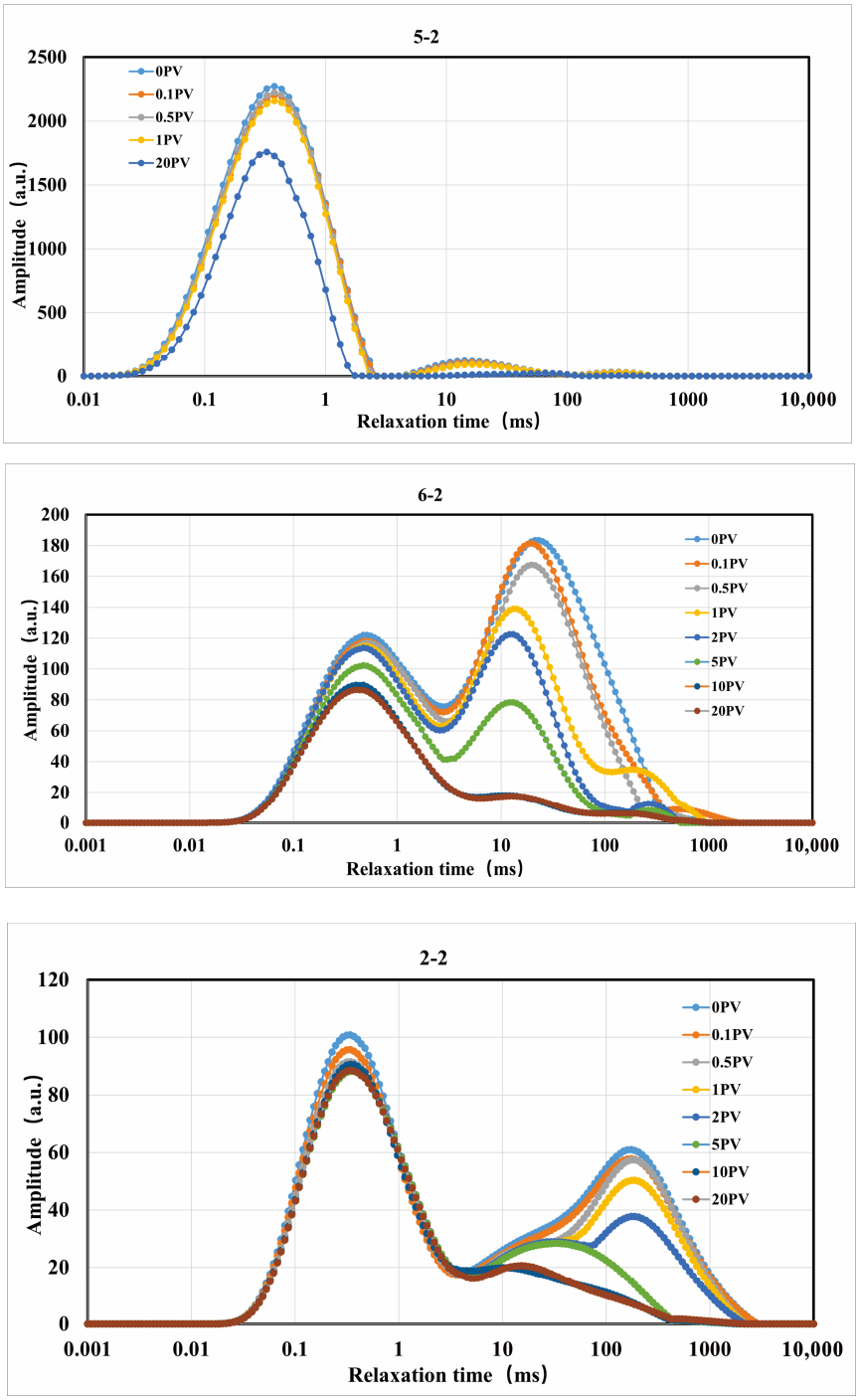


Figure 9. T2 spectrum variation of rock samples during displacement under constant effective stress conditions.

Under constant injection pressure conditions, the oil displacement efficiency for low-permeability, medium-permeability, and fractured cores is 36.55%, 40.23%, and 47.05%, respectively (Figure 10). The presence of fractures significantly enhances the displacement efficiency by providing additional pathways for the CO_2 to penetrate the core, thereby increasing the swept volume and contact area with the oil. Under variable injection pressure conditions, the oil displacement efficiency for low-permeability, medium-permeability, and fractured cores is 49.30%, 59.70%, and 43.45%, respectively (Figure 11). In this scenario, medium-permeability cores exhibit the highest displacement efficiency, possibly due to more uniform fluid flow distribution within the core. In fractured cores, fluid

may bypass certain areas due to faster flow rates along preferential paths, leading to an uneven displacement process known as "fingering" [34]. Conversely, low-permeability cores may hinder fluid movement, resulting in insufficient displacement. Under constant effective stress conditions, the oil displacement efficiency for low-permeability, medium-permeability, and fractured cores is 36.24%, 68.21%, and 36.94%, respectively (Figure 12). The medium-permeability cores again show the highest efficiency. Fractures do not enhance the displacement efficiency in this case, possibly because the applied confining pressure during displacement leads to fracture closure. This closure reduces the permeability of the rock samples, thereby limiting the efficiency of CO_2 displacement. The mechanics of fracture closure involve the compression of the rock matrix around the fractures, which decreases the aperture and increases the flow resistance. This phenomenon is crucial in understanding the variable impact of fractures on oil displacement under different stress conditions [35,36]. Compared with similar studies [31,37], the CO_2 displacement efficiency observed in this study is consistent with other experimental reports, confirming the effectiveness of our experimental design and the reliability of our results.

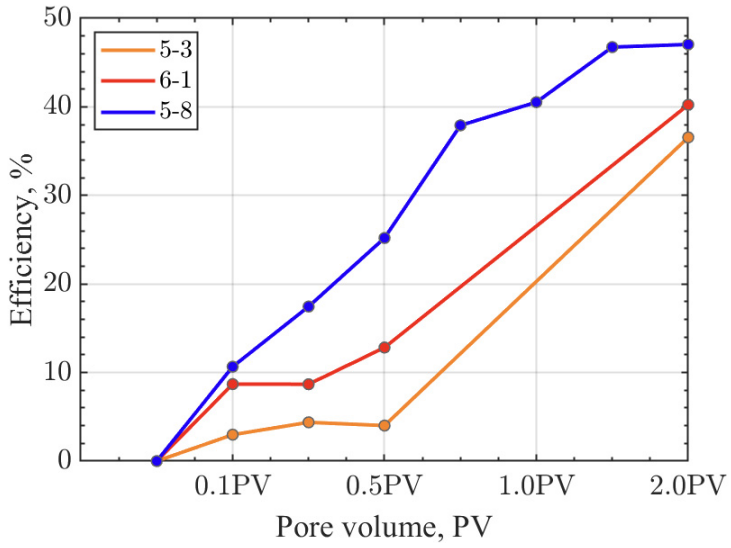


Figure 10. Displacement efficiency of different rock samples during displacement under constant injection pressure conditions.

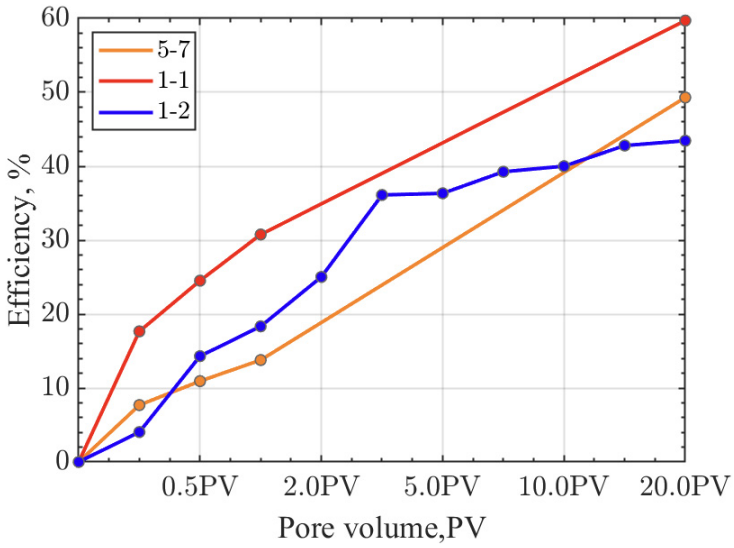


Figure 11. Displacement efficiency of different rock samples during displacement under variable injection pressure conditions.

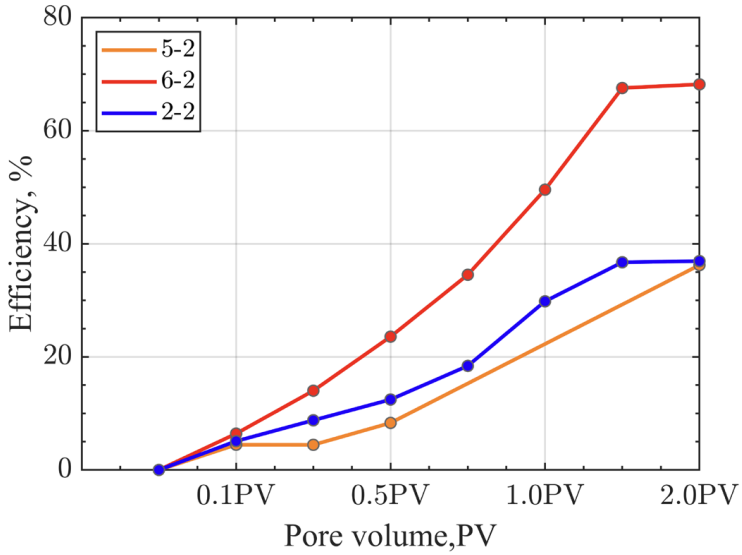


Figure 12. Displacement efficiency of different rock samples during displacement under constant effective stress conditions.

3.3. Recovery Stages

Based on the recovery rate, the CO_2 oil displacement recovery stages are divided into early, middle, and late stages. The recovery rates of rock samples under different gas injection conditions vary significantly, with the overall displacement efficiency being higher during the middle stage (Figure 13).

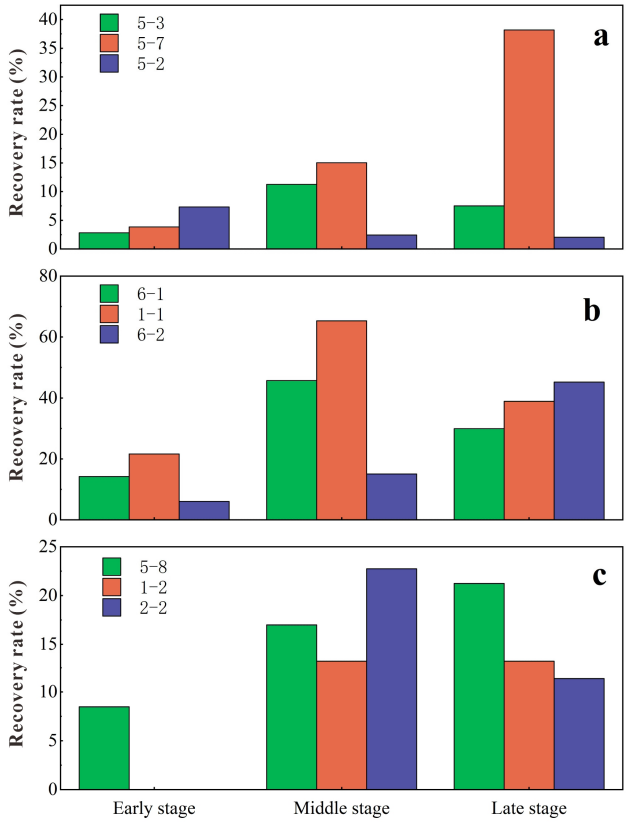


Figure 13. CO_2 oil displacement recovery stages: (**a**) low-permeability samples; (**b**) medium-permeability samples; (**c**) high-permeability samples.

The displacement process of fractured rock samples was closely monitored. Based on the gas–oil ratio and recovery degree at the outlet section of the fractured rock samples, the CO_2 oil displacement exhibited "no gas detected" and "gas detected" stages. Depending on the injection conditions, the "gas detected" stage can include various sub-stages, such as "very little gas, gas breakthrough, large gas channeling, gas fluctuation" (Figures 14–16). Specifically, during the "no gas detected" stage, the gas–oil ratio is zero, and the recovery degree is zero under both variable injection pressure and constant effective stress conditions. In the range of 0.1–0.5 PV under constant effective stress conditions, the gas–oil ratio is 85, which is classified as the very little gas stage. Under constant and variable injection pressure conditions, the gas breakthrough stage begins at 0.1 PV of injection volume and ends at 2 PV. During this stage, the recovery degree ranges from 0 to 40%, and the gas–oil ratio ranges from 100 to 4000. The large gas channeling stage has a gas–oil ratio greater than 4000. Although the displacement stages vary for different cores, the gas–oil ratio is in the breakthrough stage within the range of 0–2 PV. During this stage, the gas–oil ratio of different cores shows significant variation and follows the trend of the fitted line ($y = 1141.18x - 13.76$, $R^2 = 0.93$) (Figure 17).

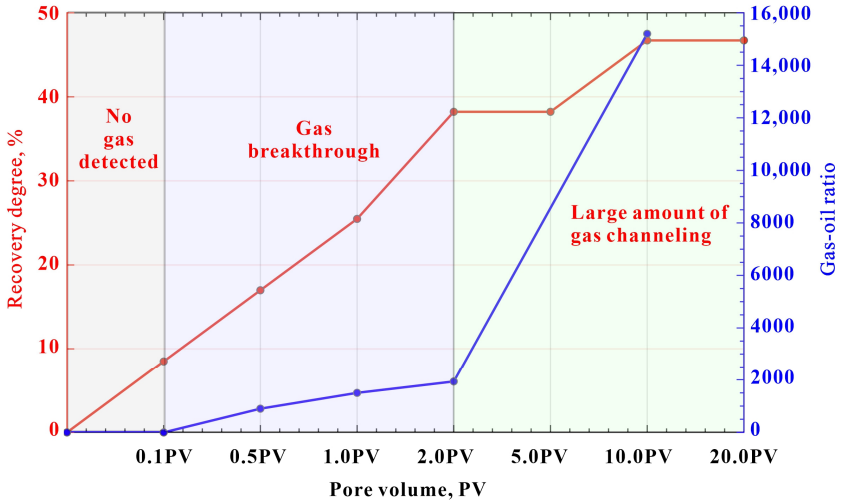


Figure 14. Recovery degree and gas–oil ratio of sample 5-8 during displacement under constant injection pressure conditions.

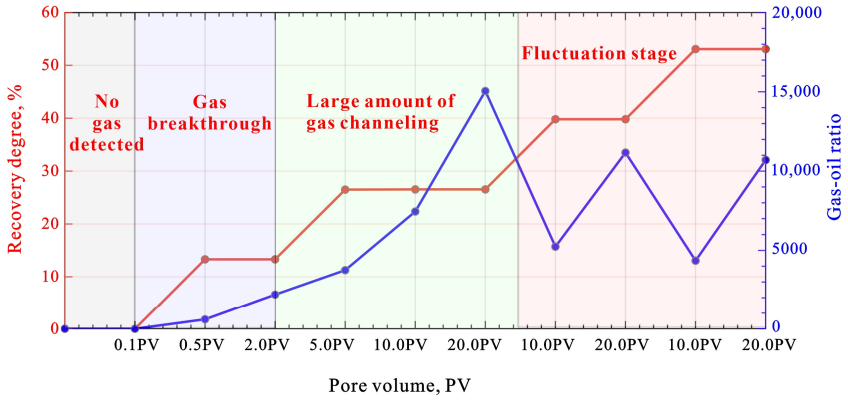


Figure 15. Recovery degree and gas–oil ratio of sample 1-2 during displacement under variable injection pressure conditions.

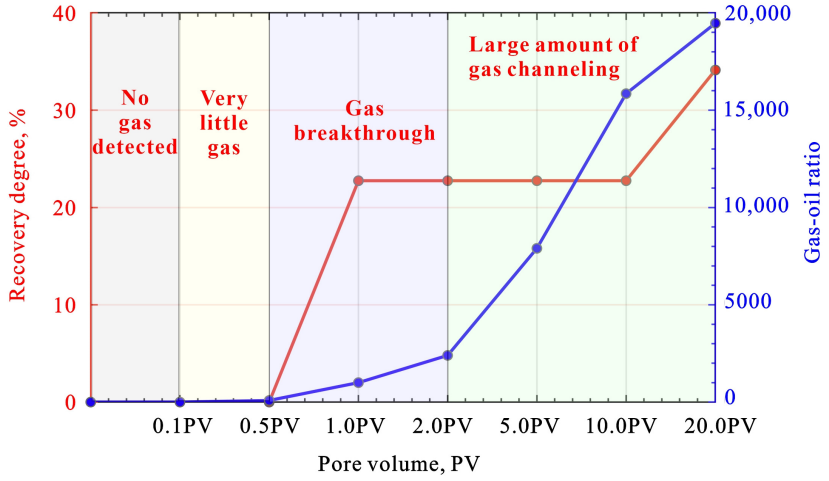


Figure 16. Recovery degree and gas–oil ratio of sample 2-2 during displacement under constant effective stress conditions.

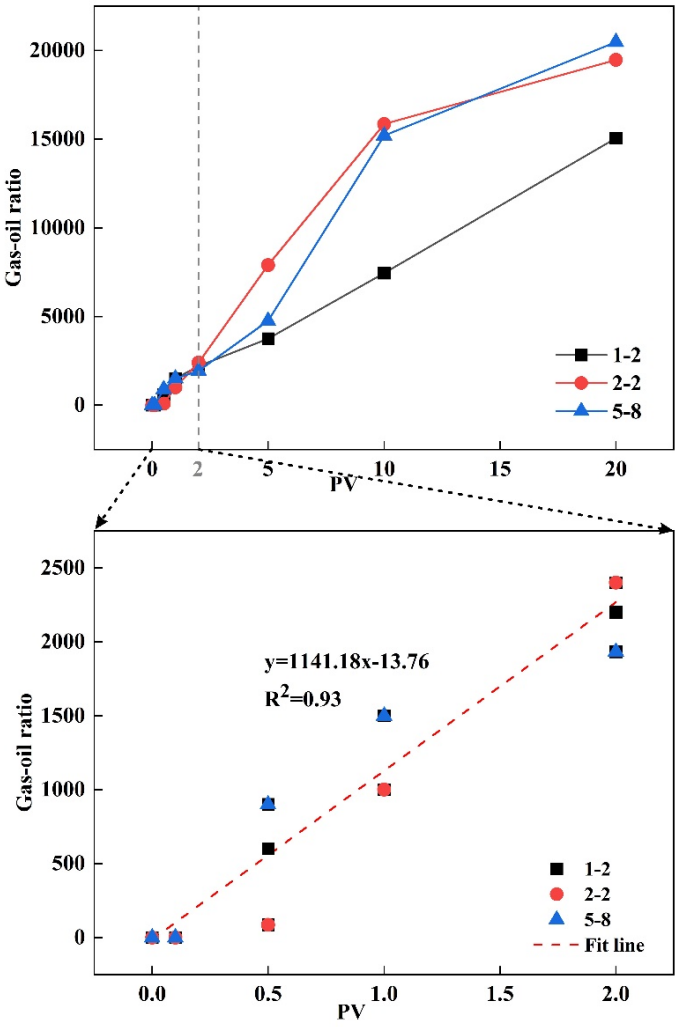


Figure 17. Relationship between gas–oil ratio and gas injection volume during the gas breakthrough stage under different displacement conditions for various samples.

4. Conclusions

In this study, displacement experiments were conducted on sandstone cores from the Chang 6 reservoir in the Huaziping area using a multifunctional core displacement apparatus and Nuclear Magnetic Resonance (NMR) technology. The CO_2 displacement process was dynamically monitored under constant-pressure, variable-pressure, and constant effective stress conditions. Injection stages were quantitatively categorized, providing valuable guidance for improving recovery rates. The conclusions obtained from this study are as follows:

(1) The distribution characteristics of rock sample pores are a key factor affecting CO_2 displacement efficiency. Under the same conditions, rock samples with a higher proportion of large pores exhibit higher CO_2 displacement efficiency. This finding suggests that reservoir characterization focusing on pore structure could be a valuable predictor of CO_2-EOR success.

(2) Fractures can contribute to improving CO_2 displacement efficiency. However, the applied confining pressure during displacement can cause fracture closure, reducing the permeability of the rock samples and the efficiency of CO_2 displacement. In field applications, injection pressure needs to be carefully managed to optimize fracture utilization.

(3) Based on the recovery rate, the CO_2 oil displacement recovery stages are divided into early, middle, and late stages. The recovery rates of rock samples under different gas injection conditions vary significantly, with the overall displacement efficiency being higher during the middle stage. Based on the gas–oil ratio and recovery degree at the outlet section of fractured rock samples, the CO_2 oil displacement process can be divided into five stages: no gas detected, very little gas, gas breakthrough, large gas channeling, and gas fluctuation. Although the displacement stages differ among rock samples, the breakthrough stage tends to occur within the 2 PV range. The identification of distinct displacement stages, particularly gas breakthrough within the 2 PV range, provides a framework for monitoring and adjusting CO_2-EOR operations in the field.

To apply these findings to field-scale operations, careful consideration must be given to the scalability of the experimental conditions and the inherent heterogeneity of reservoir properties. The controlled laboratory environment may not fully capture the complexities of subsurface conditions, such as variations in stress, temperature, and fluid interactions across larger spatial scales. Therefore, while our results suggest promising strategies for enhancing CO_2-EOR efficiency, they must be validated through pilot tests and cautiously scaled up, taking into account the unique characteristics and constraints of each reservoir.

Author Contributions: Y.Z. conducted the experiments and drafted the manuscript. X.W. analyzed the experimental results. Y.K. provided the core samples and partial funding. C.G. designed the experiments and helped with manuscript editing. Q.H. sought funding. C.L. supervised the experiment and reviewed and edited the manuscript. All authors have read and agreed to the published version of the manuscript.

Funding: This work was supported by the China National Science Foundation (grant Nos. U2244215, U2344226, 42372286, 42002255), the China Geological Survey Project (DD20221819), and the Fundamental Research Funds of the Chinese Academy of Geological Sciences (JKY202413, JKYQN202306).

Data Availability Statement: Data are available from the corresponding author upon reasonable requests.

Conflicts of Interest: Author Yulong Kang was employed by the company Shaanxi Yanchang Petroleum (Group) Co., Ltd. The remaining authors declare that the research was conducted in the absence of any commercial or financial relationships that could be construed as a potential conflict of interest.

References

1. Sambo, C.; Liu, N.; Shaibu, R.; Ahmed, A.A.; Hashish, R.G. A technical review of CO_2 for enhanced oil recovery in unconventional oil reservoirs. *Geoenergy Sci. Eng.* **2023**, *221*, 111185. [CrossRef]
2. IEA. *World Energy Outlook 2023*; IEA: Paris, France, 2023. Available online: https://www.iea.org/reports/world-energy-outlook-2023 (accessed on 30 August 2024).
3. IEA. *The Future of Petrochemicals*; IEA: Paris, France, 2018. Available online: https://www.iea.org/reports/the-future-of-petrochemicals (accessed on 30 August 2024).
4. Zhou, W.; Niu, M.-Y.; Luo, W.-J.; Liu, X.-T. Research Progress on Enhanced Oil Recovery by CO_2 Flooding in Low Permeability Reservoirs. In Proceedings of the International Field Exploration and Development Conference, Wuhan, China, 20–22 September 2023; pp. 343–366.
5. Syed, F.I.; Muther, T.; Van, V.P.; Dahaghi, A.K.; Negahban, S.J.F. Numerical trend analysis for factors affecting EOR performance and CO_2 storage in tight oil reservoirs. *Fuel* **2022**, *316*, 123370. [CrossRef]
6. Farajzadeh, R.; Eftekhari, A.A.; Dafnomilis, G.; Lake, L.; Bruining, J. On the sustainability of CO_2 storage through CO_2–Enhanced oil recovery. *Appl. Energy* **2020**, *261*, 114467. [CrossRef]
7. Al-Abri, H.; Pourafshary, P.; Mosavat, N.; Al Hadhrami, H. A study of the performance of the LSWA CO_2 EOR technique on improvement of oil recovery in sandstones. *Petroleum* **2019**, *5*, 58–66. [CrossRef]
8. Yang, Z.-P.; Liao, X.-W.; Wang, X.-C. Optimization Study of Injection-Production Parameters for CO_2 Enhanced Oil Recovery and Storage in Low Permeability Oil Reservoirs. *J. Phys. Conf. Ser.* **2023**, *2594*, 012055. [CrossRef]
9. Gong, Y.; Gu, Y.J.E. Experimental study of water and CO_2 flooding in the tight main pay zone and vuggy residual oil zone of a carbonate reservoir. *Energy Fuels* **2015**, *29*, 6213–6223. [CrossRef]
10. Wang, S.; Kadhum, M.J.; Chen, C.; Shiau, B.; Harwell, J.H. Development of in situ CO_2 generation formulations for enhanced oil recovery. *Energy Fuels* **2017**, *31*, 13475–13486. [CrossRef]
11. Zhou, X.; Yuan, Q.; Zhang, Y.; Wang, H.; Zeng, F.; Zhang, L. Performance evaluation of CO_2 flooding process in tight oil reservoir via experimental and numerical simulation studies. *Fuel* **2019**, *236*, 730–746. [CrossRef]
12. Han, B.; Cui, G.; Wang, Y.; Zhang, J.; Zhai, Z.; Shi, Y.; Yan, F.; Li, W. Effect of fracture network on water injection huff-puff for volume stimulation horizontal wells in tight oil reservoir: Field test and numerical simulation study. *J. Pet. Sci. Eng.* **2021**, *207*, 109106. [CrossRef]
13. Liu, P.; Zhang, X. Enhanced oil recovery by CO_2–CH_4 flooding in low permeability and rhythmic hydrocarbon reservoir. *Int. J. Hydrogen Energy* **2015**, *40*, 12849–12853. [CrossRef]
14. Abedini, A.; Torabi, F. On the CO_2 storage potential of cyclic CO_2 injection process for enhanced oil recovery. *Fuel* **2014**, *124*, 14–27. [CrossRef]
15. Li, S.; Qiao, C.; Zhang, C.; Li, Z. Determination of diffusion coefficients of supercritical CO_2 under tight oil reservoir conditions with pressure-decay method. *J. CO_2 Util.* **2018**, *24*, 430–443. [CrossRef]
16. Li, H.-B.; Yang, Z.-M.; Li, R.-S.; Zhou, T.-Y.; Guo, H.-K.; Liu, X.-W.; Dai, Y.-X.; Hu, Z.-G.; Meng, H. Mechanism of CO_2 enhanced oil recovery in shale reservoirs. *Pet. Sci.* **2021**, *18*, 1788–1796. [CrossRef]
17. Wang, T.; Wang, L.; Meng, X.; Chen, Y.; Song, W.; Yuan, C. Key parameters and dominant EOR mechanism of CO_2 miscible flooding applied in low-permeability oil reservoirs. *Geoenergy Sci. Eng.* **2023**, *225*, 211724. [CrossRef]
18. Zhang, Y.; Shi, L.; Ye, Z.; Chen, L.; Yuan, N.; Chen, Y.; Yang, H. Experimental Investigation of Supercritical CO_2–Rock–Water Interactions in a Tight Formation with the Pore Scale during CO_2–EOR and Sequestration. *ACS Omega* **2022**, *7*, 27291–27299. [CrossRef]
19. Su, X.; Yue, X. Mechanism study of the relation between the performance of CO_2 immiscible flooding and rock permeability. *J. Pet. Sci. Eng.* **2020**, *195*, 107891. [CrossRef]
20. Hore, P.J. *Nuclear Magnetic Resonance*; Oxford University Press: New York, NY, USA, 2015.
21. Zhang, X.; Wei, B.; You, J.; Liu, J.; Wang, D.; Lu, J.; Tong, J. Characterizing pore-level oil mobilization processes in unconventional reservoirs assisted by state-of-the-art nuclear magnetic resonance technique. *Energy* **2021**, *236*, 121549. [CrossRef]
22. Cai, M.; Su, Y.; Hao, Y.; Guo, Y.; Elsworth, D.; Li, L.; Li, D.; Li, X. Monitoring oil displacement and CO_2 trapping in low-permeability media using NMR: A comparison of miscible and immiscible flooding. *Fuel* **2021**, *305*, 121606. [CrossRef]
23. Zhou, H.; Gao, F.; Zhou, X.; Liu, H.; Guo, B. NMR T2 Spectrum of Different Types of Sandstone in the Yungang Grottoes: Study on the Conversion of Capillary Pressure by Mercury. *Prog. Geophys.* **2013**, *28*, 2759–2766. (In Chinese)
24. Zhang, T.; Tang, M.; Ma, Y.; Zhu, G.; Zhang, Q.; Wu, J.; Xie, Z. Experimental study on CO_2/Water flooding mechanism and oil recovery in ultralow-Permeability sandstone with online LF-NMR. *Energy* **2022**, *252*, 123948. [CrossRef]
25. Wei, B.; Zhang, X.; Wu, R.; Zou, P.; Gao, K.; Xu, X.; Pu, W.; Wood, C. Pore-scale monitoring of CO_2 and N_2 flooding processes in a tight formation under reservoir conditions using nuclear magnetic resonance (NMR): A case study. *Fuel* **2019**, *246*, 34–41. [CrossRef]
26. Du, Q.; Liu, X.; Wang, E.; Zuo, J.; Wang, W.; Zhu, Y. Effects of CO_2–water interaction with coal on mineral content and pore characteristics. *J. Rock Mech. Geotech. Eng.* **2020**, *12*, 326–337. [CrossRef]
27. Lin, Q.; Bijeljic, B.; Foroughi, S.; Berg, S.; Blunt, M.J. Pore-scale imaging of displacement patterns in an altered-wettability carbonate. *Chem. Eng. Sci.* **2021**, *235*, 116464. [CrossRef]

28. Cai, J.; Qin, X.; Xia, X.; Jiao, X.; Chen, H.; Wang, H.; Xia, Y. Numerical modeling of multiphase flow in porous media considering micro-and nanoscale effects: A comprehensive review. *Gas Sci. Eng.* **2024**, *131*, 205441. [CrossRef]
29. Hou, P.; Ju, Y.; Gao, F.; Wang, J.; He, J. Simulation and visualization of the displacement between CO_2 and formation fluids at pore-scale levels and its application to the recovery of shale gas. *Int. J. Coal Sci. Technol.* **2016**, *3*, 351–369. [CrossRef]
30. Massarweh, O.; Abushaikha, A.S. A review of recent developments in CO_2 mobility control in enhanced oil recovery. *Petroleum* **2022**, *8*, 291–317. [CrossRef]
31. Lang, D.J.; Lun, Z.M.; Lv, C.Y.; Wang, H.T. NMR Experimental Study on the Characteristics of CO_2 Flooding in Tight Sandstone Reservoirs. *CT Theory Appl.* **2016**, *25*, 141–147. (In Chinese)
32. Zhang, T.; Zhu, M.; Zhou, G.; Wu, J.; Yang, X.; Li, R. Experimental Study on CO_2 Flooding Characteristic in Low-Permeability Sandstone Considering the Influence of In-Situ Stress. *SPE J.* **2024**, *29*, 5636–5645. [CrossRef]
33. Luo, Y.; Zheng, T.; Xiao, H.; Liu, X.; Zhang, H.; Wu, Z.; Zhao, X.; Xia, D. Identification of distinctions of immiscible CO_2 huff and puff performance in Chang-7 tight sandstone oil reservoir by applying NMR, microscope and reservoir simulation. *J. Pet. Sci. Eng.* **2022**, *209*, 109719. [CrossRef]
34. Berge, R.L.; Berre, I.; Keilegavlen, E. Numerical Simulations of Viscous Fingering in Fractured Porous Media. *Transp. Porous Med.* **2024**, *151*, 1511–1538. [CrossRef]
35. Qin, S.; Li, J.; Chen, J.; Bi, X.; Xiang, H. Research on Displacement Efficiency by Injecting CO_2 in Shale Reservoirs Based on a Genetic Neural Network Model. *Energies* **2023**, *16*, 4812. [CrossRef]
36. Wu, H.; Zhang, N.; Lou, Y.; Zhai, X.; Liu, B.; Li, S. Optimization of fracturing technology for unconventional dense oil reservoirs based on rock brittleness index. *Sci. Rep.* **2024**, *14*, 15214. [CrossRef] [PubMed]
37. Ren, J.; Xiao, W.; Pu, W.; Tang, Y.; Bernabé, Y.; Cheng, Q.; Zheng, L. Characterization of CO_2 miscible/immiscible flooding in low-permeability sandstones using NMR and the VOF simulation method. *Energy* **2024**, *297*, 131211. [CrossRef]

Disclaimer/Publisher's Note: The statements, opinions and data contained in all publications are solely those of the individual author(s) and contributor(s) and not of MDPI and/or the editor(s). MDPI and/or the editor(s) disclaim responsibility for any injury to people or property resulting from any ideas, methods, instructions or products referred to in the content.